Kinetically Distinct Three Red Chlorophylls in Photosystem I of *Thermosynechococcus elongatus* Revealed by Femtosecond Time-Resolved Fluorescence Spectroscopy at 15 K

Yutaka Shibata,* Atsushi Yamagishi, Shunsuke Kawamoto, Tomoyasu Noji, and Shigeru Itoh

Division of Material Science (Physics), Graduate School of Science, Nagoya University, Furo-cho, Nagoya 464-8602, Japan

Received: October 7, 2009; Revised Manuscript Received: December 22, 2009

Time-resolved fluorescence spectra of photosystem I (PS-I) trimeric complex isolated from a thermophilic cyanobacterium, *Thermosynechococcus* (*T.*) *elongatus*, were observed at 15 K over the time range from 100 fs to a few nanoseconds under P700-oxidized condition and 10 ps to a few nanoseconds under P700-reduced condition. Global-fitting analysis of the data of P700-oxidized condition revealed the existence of three kinetically different red chlorophylls (Chls) having the energy-transfer times to $P700^+$ of 6.1 ps ($C_{6.1\ ps}$), 140 ps ($C_{140\ ps}$), and 360 ps ($C_{360\ ps}$). According to the spectral shape of DAS, $C_{6.1\ ps}$, $C_{140\ ps}$, and $C_{360\ ps}$ were assigned to the previously reported red Chls with the absorption maxima at 715 nm (C715), 710 nm (C710), and 719 nm (C719), respectively. In PS-I containing $P700^+$, ca. 60 Chls funnel the excitation energy into $C_{6.1\ ps}$ in a subpicosecond time region at 15 K. The analysis of the present data together with the conclusions of the previous reports revealed that in PS-I containing a neutral P700 the direct energy transfer from the bulk Chls to P700 seems to dominate the energy-flow process. Simulation of the energy-transfer time to $P700^+$ based on Förster theory suggested the dimeric Chls A32-B7 and A33-A34 as the most probable candidates for $C_{140\ ps}$ (C710) and $C_{360\ ps}$ (C719), respectively. $C_{6.1\ ps}$ (C715) was tentatively assigned to the dimeric Chl B24-B25 or A26-A27, for which the fastest energy transfer to $P700^+$ was predicted from the simulation. However, the estimated energy-transfer times to $P700^+$ for these dimeric Chls were 44−46 ps, which were still much slower than the observed value of 6.1 ps. A theoretical framework beyond the standard Förster theory might be required in order to account for the severe deviation.

Introduction

Photosystem I (PS-I) is one of the two photosystems in the oxygenic photosynthesis of plants and cyanobacteria.[1,2] Ninety-six chlorophyll (Chl)-*a*'s are involved in a cyanobacterial PS-I complex. X-ray crystallographic studies have shown that these Chl-*a* molecules are approximately divided into two domains;[3,4] one contains about ninety pigments located at the peripheral part of the complex, which function as light-harvesting antennae. The other domain consists of 6−8 Chl-*a* molecules located in the central region, which are the part of the electron-transfer chain. The two Chls at the center, one of which is a $C13^2$ epimer of Chl-*a* called Chl-*a*′,[3,5] are candidates for the primary electron donor called P700.

Pigments in PS-I are densely packed and strongly interact with each other. Because of such strong interactions, the elementary energy-transfer steps among individual molecules are extremely rapid and might take place in a coherent manner. Accordingly, the elementary steps are hardly observable even with a femtosecond time resolution. What is observable is the energy-transfer dynamics among groups of Chl-*a* molecules, which have often been called "compartments".[6,7] A "compartment" is an ensemble of pigments, the dynamic processes within which are too fast to be resolved by the experimental setup being used. Although great efforts have been made to elucidate the light-harvesting kinetics in PS-I, no general consensus has been achieved. It is still under debate whether the light-harvesting kinetics in PS-I is trap-limited[8−10] or transfer-to-trap limited.[11−13] The elucidation of the light-harvesting kinetics in PS-I is challenging because it requires a deep and accurate understanding of the excited-state dynamics in densely packed and strongly coupled pigment system. The issue is further complicated by the existence of the red-most absorbing states, which are specific to PS-I.

It is well-known that there are several antenna states that have excitation-energy levels much lower than that of P700. These states are considered to be composed of specific sets of Chl-*a* molecules, which we designate red Chls hereafter. They might have crucial influence on the overall light-harvesting dynamics in PS-I. The physiological role of red Chls has not yet been clarified. PS-Is of some organisms do not contain red Chl. It has been suggested that red Chls consist of 7−11 molecules of Chl-*a* based on the deconvolution analyses of the absorption spectra of PS-I at cryogenic temperature[14] and spectral hole-burning studies.[15,16] Such analyses also suggested the coexistence of several spectrally different red Chls with absorption peak wavelengths of 706 nm (C706) and 714 nm (C714) in PS-I of *Synechocystis* PCC 6803[15,17] and 710 nm (C710), 715 nm (C715), and 719 nm (C719) in PS-I of *Thermosynechococcus* (*T.*) *elongatus*.[16] It has not yet been clarified which Chl-*a* molecules (or possibly sets of Chls) in the available X-ray structure of PS-I are responsible for the red-most absorption bands.

Several candidates for red Chls have been proposed so far.[13,18−21] All of these candidates consist of dimeric or trimeric Chls. The strong excitonic and charge-transfer interactions between the Chls in the dimer or trimer are considered to be the main cause of the red shift of their absorption spectra. Spectral hole-burning experiments have suggested that all red

* To whom correspondence should be addressed. Tel/Fax: 81-52-789-2883. E-mail: yshibata@bio.phys.nagoya-u.ac.jp.

10.1021/jp909583r
Published on Web 02/08/2010

Chls exhibit very strong electron−phonon couplings and large permanent-dipole changes upon excitation.[15,16,22] These findings suggested that the red shift of the excited state of red Chl is significantly contributed from the charge-transfer interaction between Chl molecules. The assignment of red Chls to dimeric or trimeric Chls is thus consistent with the results of the hole-burning studies. The spectral properties of C719 in PS-I of *T. elongatus* are sensitive to the decomposition of the trimeric form of PS-I, suggesting its proximity to the interfacial region of the monomer units in the trimeric PS-I.[14,15]

Although the spectral properties of red Chls are well documented, the studies of their kinetic aspects are limited.[17,23,24] Lowering the temperature is often useful to reveal the low-lying states in photosynthetic pigment systems, such as red Chls in PS-I. At cryogenic temperature, the uphill energy transfer from a lower-energy to a higher-energy state is largely suppressed. This results in a unidirectional excitation-energy flow and drastically simplifies the light-harvesting kinetics. Pålsson et al. have demonstrated that the relative fluorescence quantum yield of PS-I drastically increased upon lowering the temperature down to 50 K because of the suppression of the uphill energy transfer from red Chls to P700.[25] We have previously shown that lowering the temperature below 77 K slowed down the energy transfer in photosystem II (PS-II) .[26] Owing to the slowed energy-transfer rates, we could observe the light-harvesting dynamics in PS-II in detail.

We investigated here for the first time the femtosecond time-resolved fluorescence dynamics of PS-I from a thermophilic cyanobacterium, *T. elongatus*, at 15 K. The fluorescence up-conversion technique and the streak-camera setup were used to observe the sensitivity-corrected time-resolved fluorescence spectra in the 100 fs to a few nanoseconds time region. Combination of the up-conversion with a streak-camera setup was previously reported by Kennis et al. in the study of the fluorescence dynamics of PS-I at room temperature.[27] Basically, we applied the same method[28,29] to the study of fluorescence dynamics at cryogenic temperature. The main goal of this paper is to characterize the pathway of energy flow in PS-I, particularly through red Chls.

We compared the fluorescence dynamics between PS-I with neutral and oxidized P700 forms. It is known that at room temperature P700 in its oxidized form ($P700^+$) quenches the fluorescence of PS-I as effectively as the neutral P700.[23] $P700^+$ has been known to have a broad absorption band beyond 800 nm,[25,30] which is similar to the spectrum of an oxidized Chl in a solution.[31,32] Since the absorption spectrum of $P700^+$ has a considerable spectral overlap with a fluorescence band of red Chls, an irreversible energy transfer from red Chls to $P700^+$ has been considered responsible for the effective fluorescence quenching by $P700^+$.[23]

The present study revealed that the fluorescence from red Chls is quite effectively quenched even at cryogenic temperature when P700 is in its cation form. The results suggested the coexistence of three kinetically different red Chls having significantly different energy-transfer rates to $P700^+$. Energy funneling into one red Chl was found to be extremely fast, suggesting that light harvesting took place in a coherent manner rather than by step-by-step migrations among pigments. We propose a model of the light-harvesting pathway in PS-I at cryogenic temperature according to the present findings. The energy-transfer rates from the red Chls to $P700^+$ were analyzed on the basis of Förster theory. The analysis enabled us to examine the validity of the red Chl candidates proposed so far.

Materials and Methods

The PS-I trimer sample was purified from *T. elongatus* as described previously[33] with slight modifications. According to Kawakami et al.,[34] a TOYOPEARL DEAE 650 S column was used to purify the PS-I trimer from the solubilized thylakoids. Maintenance of the PS-I-trimeric form was confirmed by the blue-native gel electrophoresis. The purified PS-I trimer was dissolved in a 25 mM tricine-NaOH buffer of pH 7.5 containing 0.03% *n*-dodecyl-β-maltoside, 50 mM NaCl, 35 mM sodium ascorbate and 7.2 μM 1-methoxy phenazine methosulfate. In the case of measurements at room temperature, the solution was sealed in an optical cell with an optical-path length of 2 mm. The solution was continuously stirred by using a micromagnetic stirrer to prevent photodamage. The change in the absorption spectrum was negligible even after measurements for several hours in this condition.

For the measurements at cryogenic temperature, the solution was mixed with twice the volume of glycerin and contained in a copper sample holder. The solution was contained in the space between two acrylic windows spaced by an o-ring. The sample holder was fixed on the cold head of a closed-cycle refrigerator system (Model V202C5L, Daikin Industries Ltd., Osaka) and cooled down to 15 K. The sealed sample solution remained clear even at cryogenic temperature. After a typical 15-min data accumulation with a 2-mW excitation power, the signal was decreased by about 5%. Possibly, spectral hole burning at the excitation wavelength of 430 nm is responsible for the bleaching. We confirmed that the time profiles were not affected by the decrease in the signal. We measured the fresh sample position after each one-hour data accumulation by moving the sample position.

The fluorescence up-conversion and streak-camera set-ups are basically the same as those described in the previous studies.[28,29] The frequency-doubled light at 430 nm from a Ti:sapphire laser (MaiTai; Spectra-Physics, Mountain View) with a repetition rate of 80 MHz was used as the excitation source for both set-ups. The excitation power was 2 mW (25 pJ/pulse). The beam diameter at the focal plane was roughly estimated to be 40 μm, and the excitation power per unit area was ca. 160 W/cm^2. The FWHMs of the instrumental response functions (IRF) were 160 fs and 19 ps for the up-conversion and the streak-camera set-ups, respectively. The wavelength-dependent sensitivity of the system was corrected by measuring the emission spectrum of a standard lamp by the streak camera. Owing to the shared optical configurations of the excitation and collection of the fluorescence by the up-conversion and streak-camera set-ups, the sensitivity-corrected time-resolved fluorescence spectrum could be obtained over a wide temporal range from 100 fs to 10 ns through the global analysis of the data obtained from the two set-ups.

To avoid the photoaccumulation of the oxidized P700 in PS-I during the measurement, the excitation power should be kept at a very low level. However, a rather high excitation power was required to achieve satisfactory data qualities in the up-conversion measurement. Therefore, the fluorescence dynamics with the neutral P700 could be obtained only from the streak-camera setup. The 2-MHz sampling rate of the streak camera did not allow to detect 78/80 of the fluorescence excited by the 80 MHz Ti:sapphire laser. Therefore, we used a 1-MHz diode laser at 405 nm at low excitation power to maintain the neutral P700 at the expense of the time resolution. The fwhm of IRF in this case was broadened to 64 ps due to the broad pulse width of ca. 50 ps.

To increase the fraction of the neutral P700, we prepared the PS-I sample in which all the Fe−S centers were prereduced by

the treatment reported by Heathcote et al.;[35] an aliquot of sodium dithionite was added to the sample solution contained in the optical cell, and the solution was illuminated with 75 000-lx white light from a halogen lamp at 4 °C. After a 1-min illumination, the solution was rapidly cooled by immersion into a liquid-nitrogen bath. This treatment was reported to cause prereductions of all the Fe−S centers and probably a slight prereduction of A_1. The sample cell was then transferred into a He-flow type cryostat (CF1204, Oxford Instruments, Eynsham) precooled down to 50 K. Hereafter, we refer to the samples with and without the above treatment as "PS-I-FX_{red}" and "PS-I-FX_{ox}", respectively.

The fluorescence time-profile data were analyzed by the global-fitting procedure. Wavelength-time 2D images obtained by the streak camera were divided into subimages having the wavelength width of 10 nm. The signal intensity in each subimage was then integrated along the wavelength axis to give the averaged fluorescence time profile. We fitted the time profiles thus obtained from the streak-camera measurement and those from the up-conversion measurement to the model function

$$F(t) = [F_0 + A_0\theta(t)\sum_{i=1}^{N} A_i \exp(-t/\tau_i)] \otimes \mathrm{IRF}(t) \quad (1)$$

Here, F_0 is the parameter adjusting the dark-count level, N is the number of the components, and $\theta(t)$ is the Heaviside-step function. The symbol ⊗ designates the convolution and IRF(t) is the instrumental response function. IRFs were assumed to be Gaussians that fit to the observed time profiles of the laser scattering. A_0 is the parameter adjusting the difference in the sensitivity of detection between the streak-camera and up-conversion setups. Since the wavelength-dependent sensitivity of the streak-camera system was canceled out by the correction, A_0 for the data from the streak camera was set to unity. We fitted the data under the constraint in which the parameters A_i and τ_i took the same values in the data from the streak-camera and the up-conversion set-ups monitored at the same wavelength. Further, the values of τ_i were constrained to take the same values among the time profiles at different monitoring wavelengths. After this global fitting, we obtained the decay-associated spectra (DAS), which are the plots of A_i against the monitoring wavelengths.

Results

Figure 1 shows the time-wavelength 2D images of the fluorescence dynamics of PS-I at 15 K obtained by the streak-camera setup. Panels A and B show the fluorescence dynamics of PS-I-FX_{ox} with a 2-mW excitation and PS-I-FX_{red} with a 2-μW excitation, respectively. Both panels show the main fluorescence band at around 735 nm emitted from the red Chls. The peak wavelength shifted toward the longer wavelength side in PS-I-FX_{red}. Despite a much lower S/N ratio for the data in panel B due to the very low excitation power, the fluorescence decay was significantly slowed down by the reduction of Fe−S centers that kept P700 to be in its neutral form. The prereduction of Fe−S centers also caused a time-dependent shift of the red Chl fluorescence band from 730 to 745 nm, which was absent in Figure 1A. The time-dependent shift is clear in the insets of Figure 1 and indicates the energy-transfer process from pigments emitting at around 730 nm to those emitting at around 745 nm.

We interpret the slower fluorescence decay for PS-I-FX_{red} to be due to the increased fraction of P700 remaining in its neutral

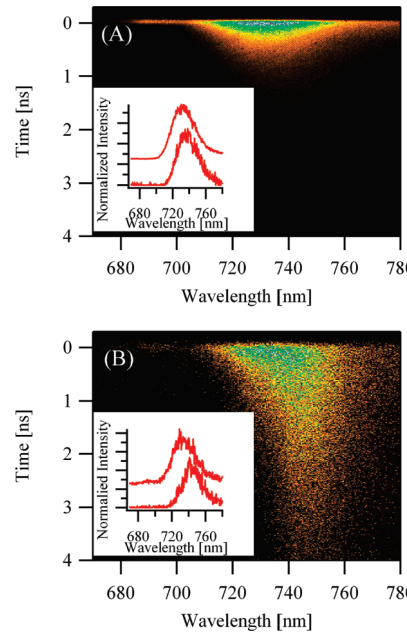

Figure 1. Wavelength-time 2D images of the fluorescence dynamics of PS-I-FX_{ox} with 2-mW excitation power (A) and PS-I-FX_{red} with 2-μW excitation power (B) at 15 K observed by a streak-camera setup. The excitation wavelength was 430 nm. The detected fluorescence signal increases in the order shown by the colors orange, yellow, green, and blue. Insets show the fluorescence spectra averaged over the time range from 0 to 100 ps (upper curves) and from 800 to 900 ps (lower curves).

form. The molar fraction of the P700 neutral form can be roughly estimated to be $k_{CR}/(k_{exc} + k_{CR})$, where k_{CR} and k_{exc} are the charge-recombination rate to the P700 ground state and the excitation rate of P700, respectively. It has been reported that the charge-recombination rate k_{CR} in a cyanobacterial PS-I is accelerated about 10 times from $4.5-8.3 \times 10^3$ to 5.0×10^4 s^{-1} upon prereduction of the Fe−S centers.[36] The excitation rate k_{exc} of P700 can be estimated from the molar-extinction coefficient 90 mM^{-1} cm^{-1} for Chl-a at 430 nm multiplied by 96, the number of the Chl-a molecules per P700, and the value of the beam diameter of 40 μm at the focal plane. k_{exc} with the excitation power of 2 mW and 2 μW were estimated to be 1.2×10^7 and 1.2×10^4 s^{-1}, respectively. Thus, when PS-I-FX_{ox} is excited by the 2 mW laser pulse at 430 nm, practically all the P700 in the excited volume is in the cation form. When PS-I-FX_{red} is excited by the 2 μW laser power, on the other hand, more than 80% of P700 is estimated to remain in the neutral form. This situation was confirmed because the fluorescence decay for PS-I-FX_{ox} measured at the excitation power of 2 μW was faster than that for PS-I-FX_{red} shown in Figure 1B (data not shown). The result clearly indicated that the reduction of the Fe−S centers decelerates the fluorescence lifetime. Although we did not measure the extent of P700 reduction under the measurement, the effects were consistent with the above estimation based on the kinetic parameters reported so far.[36]

We believe that the faster fluorescence decay in Figure 1A is not due to the singlet−singlet annihilation by the intense excitation laser because the excitation rate k_{exc} of 1.2×10^7 s^{-1} with the 2 mW excitation power is estimated to result in a negligible probability of the multipigment excitation in a single PS-I trimer. This was confirmed by the observation of the independence of the fluorescence time profiles from the excitation power, as shown in Figure 2. The fluorescence decay profile at 708 nm observed by the up-conversion setup was hardly

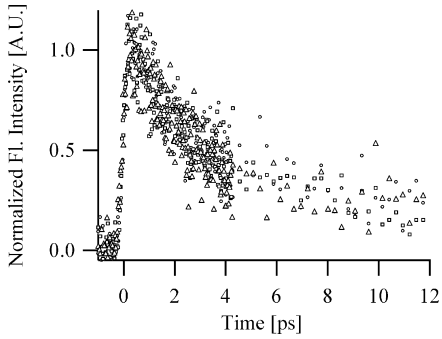

Figure 2. Fluorescence decay profiles of PS-I-FX_{ox} observed by the up-conversion setup at 708 nm with an excitation power of 1 (open circles), 2 (open squares), and 4 mW (open triangles). The excitation wavelength was 430 nm. The peak intensities were normalized to unity.

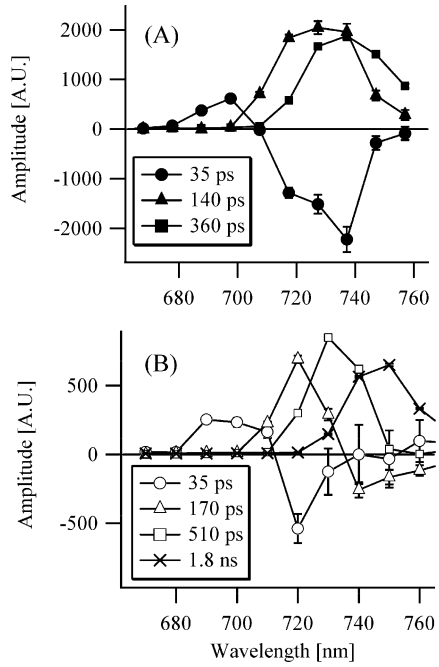

Figure 3. Decay-associated spectra of PS-I-FX_{ox} with a 2-mW excitation power and a 80-MHz repetition rate (A) and PS-I-FX_{red} with a 2-μW excitation power and a 1-MHz repetition rate (B) at 15 K in the time region beyond 10 ps. The numbers of excited Chls per P700 per pulse were estimated to be 0.15 and 0.012 for the conditions in panels A and B, respectively.

affected by the change in the excitation power from 1 to 4 mW, verifying the absence of the singlet−singlet annihilation.

In Figure 3, we compare the DAS components between PS-I-FX_{ox} (panel A) and PS-I-FX_{red} (panel B) obtained by the global fitting procedure according to eq 1. DAS for PS-I-FX_{ox} were obtained by full analysis considering the data of both the streak-camera and the up-conversion setups. In Figure 3A, we depicted the DAS components with time constants slower than 10 ps. DAS with the time constant of 35 ps are present in both sample conditions. Hereafter, we refer to this DAS component as $DAS_{35\ ps}$ according to its time constants. $DAS_{35\ ps}$ shows a positive peak at around 690 nm and a negative one at around 720 nm, reflecting the energy transfer with a time constant of 35 ps from Chls emitting at around 690 nm to the red Chls emitting at around 720 nm. The positive peak of $DAS_{35\ ps}$ had a much smaller amplitude than that of the negative peak. This might suggest a slight underestimation of the amplitude of the 35 ps decay in the 690−700 nm spectral region due to the limited time resolution of the streak-camera system. PS-I-FX_{ox} shows DAS components with time constants of 140 ps ($DAS_{140\ ps}$) and 360 ps ($DAS_{360\ ps}$) with positive peaks at around 730 and 740 nm, respectively. These two DAS components are positive over the whole spectral range. Thus, they are considered to reflect the energy transfer to the practically nonfluorescent state, that is, $P700^+$. Hereafter, we designate the energy transfer to P700 in the case of PS-I-FX_{red} or $P700^+$ in the case of PS-I-FX_{ox} as "trapping".

In the case of PS-I-FX_{red}, another slower energy-transfer process is indicated by DAS with the time constant of 170 ps ($DAS_{170\ ps}$) showing a positive peak at around 720 nm and a negative one at around 740 nm. A further red shift of the fluorescence spectrum of PS-I-FX_{red} was due to this energy-transfer process with a 170 ps time constant. DAS with a time constant beyond 1 ns were absent in PS-I-FX_{ox}, while those with a 1.8 ns time constant ($DAS_{1.8\ ns}$) were present in PS-I-FX_{red}. We interpret $DAS_{1.8\ ns}$ to correspond to the radiative relaxation process of the red Chls. The $DAS_{1.8\ ns}$ component is responsible for the much slower fluorescence decay in PS-I-FX_{red} than in PS-I-FX_{ox}.

The open circles in Figure 4 show the fluorescence time profiles of PS-I-FX_{ox} at 15 K observed by the up-conversion (panel A) and streak-camera (panel B) set-ups. In Figure 4A, we also show the fluorescence time profiles at room temperature using scattered dots for comparison. The fluorescence time profiles at room temperature essentially reproduced those in a previous report.[27] The fluorescence decays at 15 K became even faster than those observed at room temperature. The solid lines are the fitting curves according to eq 1 with six exponential components. The model curves accurately reproduced the time profiles observed by the up-conversion setup. The model curves with the same parameters, except for A_0 and F_0 in eq 1, also accurately fitted the profiles obtained by the streak-camera setup in the time region beyond 20 ps. Figure 4B shows slight deviations of the model curves in the initial phase within 20 ps, which might be attributed to the limited time resolution in the streak-camera measurement.

The time profiles observed by the up-conversion setup at 15 K decayed very rapidly in the whole observed wavelength region. This was not as expected from the results of the streak-camera measurements shown in Figures 1 and 2, which suggested a rise component of 35 ps in the fluorescence around 730 nm. Contrary to the expectation, the major part of the fluorescence decay was completed within 10 ps after the laser flash at all wavelengths measured. Thus, the present measurement revealed very fast fluorescence decays in the red-Chls spectral region with $P700^+$ at 15 K, which could not be resolved without femtosecond time resolution. The rise time of the fluorescence at around 730 nm was well within a subpicosecond time region. This showed that the excited states of red Chls were populated at a very early stage of the light-harvesting process.

Figure 5 shows DAS of PS-I-FX_{ox} over the full time range. The fastest component with the time constant of 100 fs was negative over the whole spectral range. Since the time constant of 100 fs was nearly at the limit of the time resolution of the present study, we set this time constant fixed at the value of 100 fs in the fitting iteration to avoid an erroneous conclusion. We interpreted this component as the mixture of the contribution from the internal-conversion process from the directly excited Soret band to the Q_y band and the very fast energy funneling from bulk Chls into a red Chl at 720 nm. The latter will show a spectral pattern with a positive peak at around 680 nm and a negative peak at around 720 nm. The positive peak might be

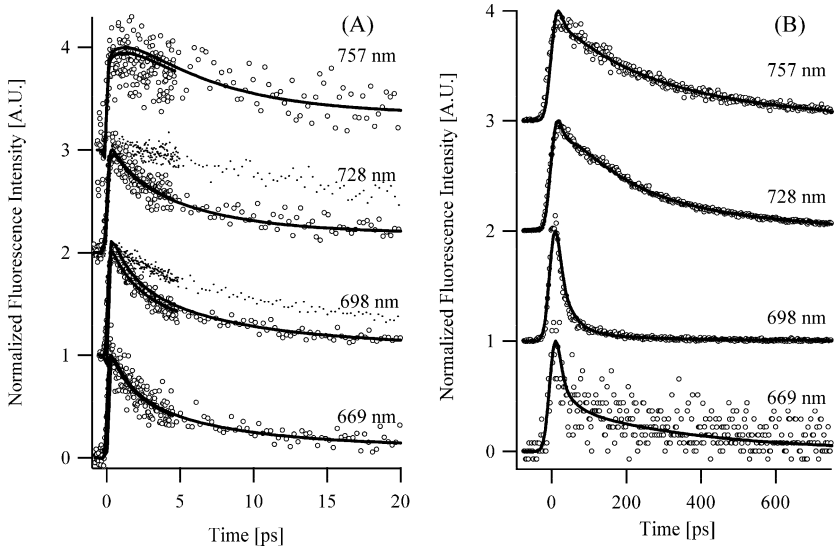

Figure 4. Open circles show the fluorescence decay profiles of PS-I-FX_{ox} at 15 K observed by the up-conversion (A) and the streak-camera (B) setups at various wavelengths. The scattered dots in panel A show the fluorescence time profiles of PS-I-FX_{ox} at room temperature. The excitation wavelength was 430 nm and the excitation power was 2 mW. Solid lines are the fitting curves according to eq 1. The time intervals of data points in decay curves in panel A are 26.7 and 267 fs before and after 5 ps, respectively. The fitting curves to both data are shown in panel A. A single global-fit analysis has given the fitting curves in panels A and B, and also the DAS in both Figures 3A and 5.

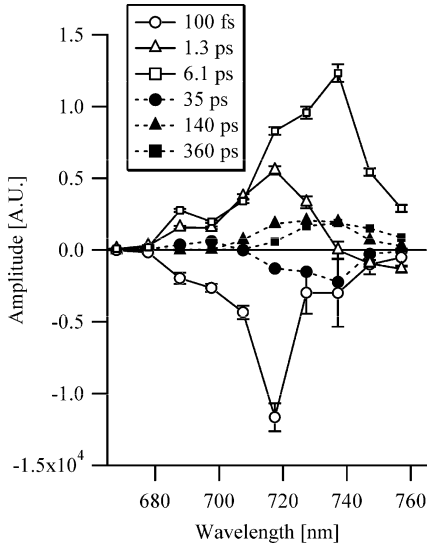

Figure 5. Decay-associated spectra of PS-I-FX_{ox} at 15 K over the full time range. The excitation wavelength was 430 nm and the excitation power was 2 mW. DAS shown by closed symbols were determined mainly from the streak-camera measurements, while those by open symbols were mainly from the up-conversion measurements.

canceled out by mixing with the internal-conversion process. The second fastest DAS component with the time constant of 1.3 ps ($DAS_{1.3\ ps}$) was interpreted to be partly due to the trapping from the band at around 720 nm. The negative peak at around 750 nm suggested that $DAS_{1.3\ ps}$ is partially contributed from the energy-transfer process from 720 to 750 nm.

DAS with the 6.1-ps time constant ($DAS_{6.1\ ps}$) has the main band at around 740 nm and is positive in the whole spectral region. $DAS_{6.1\ ps}$ indicates an unexpectedly fast 6.1-ps trapping process from the red Chl at 15 K. A small side-peak at around 690 nm in $DAS_{6.1\ ps}$ suggests a mixture of the trapping from the bulk Chls emitting at 690 nm. There are three DAS components, $DAS_{6.1\ ps}$, $DAS_{140\ ps}$, and $DAS_{360\ ps}$, showing trapping characters in PS-I-FX_{ox}. The kinetic parameters determined in the present study are summarized in Table 1.

TABLE 1: Kinetic Parameters of the Fluorescence of PS-I Samples

sample	component	time constant [ps]	peak wavelength [nm]	relative area
PS-I-FX_{ox}	$DAS_{0.1\ ps}$	0.1	720 (−)	−0.46 ± 0.12
	$DAS_{1.3\ ps}$	1.3 ± 0.12	720 (+), 760 (−)	
	$DAS_{6.1\ ps}$	6.1 ± 0.24	740 (+)	0.77 ± 0.05
	$DAS_{35\ ps}$	35 ± 5.4	690 (+), 730 (−)	
	$DAS_{140\ ps}$	140 ± 18	730 (+)	0.12 ± 0.01
	$DAS_{360\ ps}$	360 ± 25	740 (+)	0.11 ± 0.01
PS-I-FX_{red}	$DAS_{35\ ps}$	35	700 (+), 720 (−)	
	$DAS_{170\ ps}$	170 ± 14	720 (+), 740 (−)	
	$DAS_{510\ ps}$	510 ± 20	730 (+)	0.50 ± 0.02
	$DAS_{1.8\ ns}$	1800 ± 30	750 (+)	0.50 ± 0.01

Discussion

Light-Harvesting Kinetics in PS-I Containing Oxidized P700. In the present study, we observed the fluorescence dynamics of PS-I containing the oxidized primary donor $P700^+$ at 15 K over a very wide temporal range from 100 fs to a few nanoseconds. The dynamics is summarized in Table 1 and as 6 DAS components in Figure 5. According to previous studies,[23,37] we interpreted the fluorescence quenching in PS-I-FX_{ox} containing $P700^+$ to be due to the energy transfer from red Chls to $P700^+$ and the rapid relaxation to the lowest excited state of $P700^+$ after its energy acceptance. The above interpretation is supported by the present observation of the emergence of a 1.8-ns slow fluorescence decay component in PS-I by maintenance of the neutral P700 that cannot be an energy acceptor from red Chls at cryogenic temperature.

The three DAS components with trapping characters have the main bands at around 720 to 740 nm, indicating an existence of at least three kinetically different red Chls showing different energy-transfer rates to $P700^+$. Different energy-transfer rates might be partly due to the different distance from each red Chl to $P700^+$. We hereafter refer to the three red Chls as $C_{6.1\ ps}$, $C_{140\ ps}$, and $C_{360\ ps}$ according to their time constants of the energy transfer to $P700^+$. The present results are basically in line with the previous report by Byrdin et al.[23] except for the dynamics within 10 ps. $DAS_{140\ ps}$ and $DAS_{360\ ps}$ are similar to the DAS

components in their report. The presence of $DAS_{140\ ps}$ and $DAS_{360\ ps}$ that are mainly contributed from red Chls are also in good agreement with the conclusion in recent study by Slavov et al.,[24] which suggested the contributions of two red Chl pools in the fluorescence dynamics of PS-I of *T. elongates* at room temperature. The fast $DAS_{6.1\ ps}$ component was identified for the first time and shows surprisingly rapid trapping.

As shown in Figure 5, $DAS_{6.1\ ps}$ has a dominating spectral area, in contrast to the residual DAS components. This shows that the energy transfer to $P700^+$ through $C_{6.1\ ps}$ is the main pathway of the fluorescence quenching in PS-I-FX_{ox} containing $P700^+$. As shown in Figures 2, 4, and 5, the very fast rise of the fluorescence at around 720 nm indicates a rapid energy flow to $C_{6.1\ ps}$, which is mainly completed within 1 ps. $DAS_{1.3\ ps}$ suggests a slower energy-flow process of 1.3 ps to $C_{6.1\ ps}$. $DAS_{35\ ps}$ reflects the energy flow into $C_{140\ ps}$ and/or $C_{360\ ps}$. The rather slow energy-transfer time of 35 ps suggests weak coupling between the energy-donating bulk Chls and $C_{140\ ps}$ and/or $C_{360\ ps}$.

The spectral area of each trapping DAS can be a rough estimate for the relative number of the antenna Chl molecules that funnel the excitation energy into the red Chl mediating the trapping. As summarized in Table 1, the relative areas for $DAS_{6.1\ ps}$, $DAS_{140\ ps}$, and $DAS_{360\ ps}$ were estimated to be 0.77, 0.12, and 0.11, respectively. These values indicate that the 94 antenna Chls (2 Chls belonging to the special pair are excluded) in PS-I are divided into three major groups, which are assumed to contain ca. 70, 11, or 10 Chl-*a* molecules. The photon energy captured by a Chl contained in a Chl group is mainly funneled into the red Chl belonging to the same group and subsequently transferred to $P700^+$ with a respective time constant.

Recently, Slavov et al. have shown that the Chl molecules forming the part of the electron-transfer chain (they called this the "RC" compartment) emits non-negligible fluorescence at room temperature by using the picosecond-time-resolved fluorescence spectroscopy and the global analysis.[24] The species-associated spectrum of the RC compartment in their study had maximum in the 700−720-nm spectral region, and the decay time of its population was estimated to be a few picoseconds. Although the redox state of P700 in their study was different from that of PS-I-FX_{ox}, it is possible that the RC compartment contributes to the rapidly decaying fluorescence components observed in the present study at 15 K. We consider that either $DAS_{1.3\ ps}$ or $DAS_{6.1\ ps}$ contains the contribution of the RC compartment.

$DAS_{1.3\ ps}$ contains a large trapping contribution in the 700−720-nm spectral region. The peak position of $DAS_{1.3\ ps}$ is in good agreement with that of the species-associated spectrum of the RC compartment reported by Slavov et al.[24] Thus, $DAS_{1.3\ ps}$ might be the mixture of the fluorescence decay of RC and the energy-transfer from 720 to 750 nm, which happen to have the same time constant. $DAS_{6.1\ ps}$ has a small sideband at around 690 nm, suggesting a direct trapping pathway from bulk Chls to $P700^+$ without going through $C_{6.1\ ps}$. Since the sideband makes up about 10% of the whole spectral area of $DAS_{6.1\ ps}$, about 10% of the 70 Chls are suggested to directly funnel the excitation energy into $P700^+$. These 7 Chl molecules might be those forming the RC compartment.

Change in Light-Harvesting Kinetics in PS-I upon Reduction of P700. Next, we discuss the light-harvesting dynamics when P700 is maintained in the neutral form. Unfortunately, we cannot measure the fluorescence dynamics of PS-I with fully reduced P700 by the present up-conversion technique. Therefore, here, we discuss the light-harvesting dynamics in PS-I that contains the neutral P700 on the basis of the present results with a 64 ps time resolution as well as the reported results by other groups. As discussed above, the major part of the excitation energy first flows into red Chls in PS-I with $P700^+$. We can say that this does not seem to occur when P700 is in its neutral form on the basis of arguments noted in previous reports. If the excitation energy is mainly funneled into red Chls first, it cannot reach the neutral P700, which has a much higher excited state than red Chls. Accordingly, the reduction of P700 should drastically increase the fluorescence quantum yield at a cryogenic temperature. This, however, clearly contradicts a previous observation by Byrdin et al.[23] They observed the relative fluorescence yield of both P700-oxidized and -reduced PS-I samples at 295 to 5 K and suggested the increase of fluorescence yield only by a factor of 2 upon the reduction of P700 at 5 K.

Melkozernov et al.[17] measured the transient-absorption changes in PS-I containing neutral P700 of *Synechocystis* PCC6803 at 77 K and discussed the energy trapping in PS-I. Their observation showed that the rise time of the excited state of red-Chl to be 4−6 ps, much slower than that estimated here for PS-I containing $P700^+$. Since a similar red Chl composition has been suggested in PS-I from *T. elongatus* and *Synechocystis*,[15−17] the light-harvesting dynamics in PS-I from *T. elongatus* used in the present study should be similar to that from *Synechocystis*. These previous findings clearly show that the main pathway of trapping in a neutral-P700-containing PS-I is the direct energy transfer from bulk Chls to P700 without contribution of the energy transfer through red Chls.

As mentioned above, the present study, together with previous findings, shows that the energy-transfer pathway is drastically changed upon the oxidation/reduction of P700. In Figure 6, we depict a schematic model of the light-harvesting pathway in PS-I with P700 in both the oxidized (panel A) and neutral (panel B) forms. When P700 is in the oxidized form, the 94 antenna Chls seem to be divided into several groups as shown by the solid closed curves. Here, we use the term "compartment" for the group of Chls mentioned above. Three compartments contain red Chls. The excitation energy in each compartment, except for the one containing central 8 Chls including P700, is first transferred to a compartment containing a red Chl. The excitation energy is then transferred to $P700^+$ with a respective time constant. The dashed closed curves show the grouping of strongly connected compartments. When P700 is in the oxidized form, about 60 Chl molecules funnel the excitation energy into $C_{6.1\ ps}$ within 1.3 ps. There are compartments that are only weakly coupled to the compartment containing $C_{140\ ps}$ or $C_{360\ ps}$; they are responsible for the energy-transfer component expressed by $DAS_{35\ ps}$.

When P700 turns to its neutral form, reorganization of the grouping of compartments takes place. Compartments without red Chl become tightly connected to the central compartment containing P700. Then, the direct energy transfer from bulk Chls to P700 is the main path of energy flow in PS-I containing the neutral P700. The energy funneling from bulk Chls into the neutral P700 should be very rapid because it overcomes the other energy-transfer channel to the compartments containing red Chl. The residual minor part of the excitation energy is funneled into the red Chls. The excitation energy on the red Chls is either emitted as long-wavelength fluorescence or transferred to another red Chl having a lower energy level. In fact, in the present study, we observed an energy transfer from 720 to 750 nm in PS-I-FX_{red} with a time constant of 170 ps.

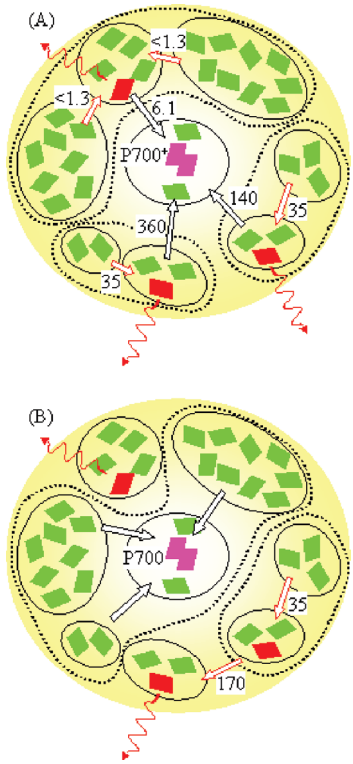

Figure 6. Schematic description of the light-harvesting pathway in PS-I containing oxidized (A) and neutral (B) P700 at 15 K. Closed squares in light green, red, and purple show the bulk Chls, red Chls, and special-pair Chls, respectively. The solid closed curves represent compartments including a set of tightly coupled Chls. The dashed closed curves represent the group of compartments connected strongly to each other. Arrows in red and black indicate the energy flow to the red Chls and to the quencher, $P700^+$ (A) or P700 (B), respectively. The number alongside each arrow represents the time constant of the energy transfer in picoseconds. The arrows of undulating lines in red show the fluorescence emission from red Chls.

The light-harvesting kinetics in PS-I is considered to be essentially temperature independent below 77 K because of the large energy gap between the bulk and red Chls, which effectively suppresses the uphill energy transfer. This forms a clear contrast to the case of PS-II, which shows a significant slowing down of the energy-transfer rate upon cooling down below 77 K.[26] On the other hand, at room temperature the fluorescence decays in the spectral region of red Chls become slower than those at cryogenic temperature as shown in Figure 4A. Thus, the energy-transfer pathway at room temperature seems somewhat different from that at cryogenic temperature, probably because of the thermally activated escape of the excitation energy from red Chls. For more accurate understanding of the energy-transfer kinetics of PS-I at room temperature, further elucidation of the kinetics at intermediate temperatures is required.

Assignment of Red Chl Species Based on the Observed Kinetics and PS-I Structure. The molecular identities of red Chls have long been argued.[19−21] Precise measurements of the absorption spectrum at cryogenic temperature have revealed the several spectrally distinct red Chls (C710, C715, and C719) in PS-I of *T. elongatus*.[16] On the basis of the peak positions of the DAS component, we assign $C_{6.1\ ps}$, $C_{140\ ps}$, and $C_{360\ ps}$ in PS-I-FX_{ox} to C715, C710, and C719, respectively. The terminal emitter in PS-I-FX_{red} is also assigned to C719. The energy-transfer process with a time constant of 170 ps observed for PS-I-FX_{red} is inferred to correspond to that from C710 to C719 based on the peak wavelength. This is consistent with the observation by Riley et al.[38] They suggested that the excitation energy on C710 is transferred to C719 with a time constant that is much slower than 5 ps.

TABLE 2: Distances to P700, Predicted Transition Dipole Magnitudes, and τ_{ET} of the Red Chl Candidates

oligomeric Chl[a]	distance to P700[b] [Å]	transition-dipole strength[c] [D]	energy-transfer time to $P700^+$ [d] [ps]
B37−B38[(i,ii,iii)]	35.4	2.67	>2300
A38-A39[(i,ii,iii)]	35.4	2.38	>2800
A32-B7[(i,ii,iii)]	28.0	5.95	>110
A33-A34[(ii,iii)]	44.9	6.02	>580
B22−B34[(iii)]	26.7	5.49	>92
A24-A35[(iii)]	27.1	5.52	>99
A10-A18[(ii)]	58.0	6.00	>5200
A12-A14[(ii)]	51.5	6.21	>1900
B9−B17[(ii)]	57.9	6.04	>4800
B24−B25[(ii)]	26.4	3.97	>46
A26-A27[(ii)]	26.6	3.95	>48
B2−B3[(iv)]	35.3	0.65	>18000
A3-A4[(iv)]	35.2	0.52	>37000
B31−B32−B33[(i)]	48.0	7.46	>510

[a] Oligomers of strongly coupled Chls suggested by [(i)]Byrdin et al.,[18] [(ii)]Damjanović et al.,[20] [(iii)]Sener et al.,[19] and [(iv)]Balaban.[21] [b] Distances between the centers of gravity of Mg atoms of the oligomeric Chl and P700. [c] Magnitudes of the transition-dipole moments estimated for the lowest excitonic states of the oligomers. [d] Lower limits of the energy-transfer times from the oligomer to $P700^+$.

In Table 2, we listed oligomeric Chls in PS-I that have been suggested to have considerably strong excitonic (and charge-transfer) interactions with the counterpart Chl-*a* in the oligomer.[19−21] Here, we used the nomenclature of Jordan et al.[3] for Chl naming. Among these oligomeric Chls, Sener et al. proposed A32-B7, A33-A34, A24-A35, and B22-B34 as the most probable candidates for the red Chl. They rejected the others because of the low transition-dipole strengths of the lowest state of the oligomer. In the study by Damjanović et al., the charge-transfer interaction as well as the excitonic interaction was taken into account. Although their simulated absorption spectrum showed little agreement with the experimental result, they estimated the effect of the surrounding protein on the site energy of each pigment. On the basis of the simulated eigenstates, they speculated that A32-B7 (partly contributed from A31 and B6), B24-B25, and A26-A27 are responsible for C719, C715, and C710, respectively. Balaban proposed that the *syn*-ligated Chl-*a* dimers, B2-B3, and A3-A4, could be candidates for the red Chls.

We tentatively assumed all of the oligomeric Chls listed in Table 2 as potential candidates for red Chls. As shown above, we experimentally identified the three kinetically distinct red Chls, $C_{6.1\ ps}$, $C_{140\ ps}$, and $C_{360\ ps}$, which have considerably different energy-transfer rates to $P700^+$. We will examine below whether the red Chl candidates listed in Table 2 can reproduce the kinetic properties determined here on the basis of the available structural information. We will simulate the energy-transfer times from each Chl-*a* oligomer in Table 2 to $P700^+$ and among the oligomers on the basis of Förster theory and compare the simulated values with the experimentally obtained one.

The energy-transfer time τ_{ET}, that is, the inverse of the rate k_{ET}, by the Förster mechanism is expressed as[39]

$$1/\tau_{ET} \equiv k_{ET} = 1.18V^2J, \quad J = \int d\nu\, F_D(\nu)A_A(\nu) \qquad (2)$$

Here, V is the excitonic interaction in cm^{-1}, and J is the spectral overlap between the fluorescence spectrum $F_D(\nu)$ of the donor and the absorption spectrum $A_A(\nu)$ of the acceptor. $F_D(\nu)$ and $A_A(\nu)$ are functions of light energy in cm^{-1}, and they are normalized so that the integrated area becomes unity. Equation 2 gives k_{ET} in ps^{-1}. In the case of the energy transfers among the red Chl candidates in Table 2 and $P700^+$, the separation between the donor and acceptor is always significantly larger than 1 nm. Therefore, V in eq 2 is appropriately given by the dipole−dipole coupling expressed as

$$V = \frac{5.04}{n^2}\left(\frac{\vec{\mu}_D \cdot \vec{\mu}_A}{r_{iDA}^3} - \frac{3(\vec{\mathbf{r}}_{DA} \cdot \vec{\mu}_D)(\vec{\mathbf{r}}_{DA} \cdot \vec{\mu}_A)}{r_{iDA}^5}\right) \qquad (3)$$

Here, $\vec{\mu}_{D/A}$ is the transition dipole moment of the donor/acceptor in the D unit, $\vec{\mathbf{r}}_{DA}$ is a vector in nanometers connecting the centers of gravity of the central Mg atoms of the donor and acceptor oligomeric Chls, and n is the refractive index of the medium.

To estimate the energy-transfer rates by eqs 2 and 3, the transition-dipole moments of the Chl-*a* oligomers were estimated by assuming the formation of the delocalized excitonic states within the oligomer. The excitonic eigenstate of each oligomer was determined by diagonalizing the interaction Hamiltonian

$$H = \begin{pmatrix} \varepsilon_1 & V_{12} & \cdots & V_{1N} \\ V_{21} & \varepsilon_2 & \cdots & V_{2N} \\ \vdots & \vdots & \ddots & \vdots \\ V_{N1} & V_{N2} & \cdots & \varepsilon_N \end{pmatrix} \qquad (4)$$

where ε_i is the site energy of the ith pigment in the oligomer and V_{ij} is the excitonic coupling between ith and jth molecules. N is the number of pigment molecules included in the oligomer. Since there has been no reliable method to estimate the site energy of each Chl-*a* in a protein, we assumed here that the site energies of all monomer pigments take the same value of 14 250 cm^{-1}. V_{ij} was calculated according to the dipole approximation given by eqution 3, which might be erroneous when the separation of the pigments is less than 1 nm.[19,40] However, we assumed here the same site energy for all of the monomers; then, the transition-dipole moment of the excitonic eigenstates is not affected by the value of V_{ij} except for the case of the trimeric Chl. In Table 2, we list the magnitude of the estimated transition-dipole moment of the lowest eigenstate of each oligomeric Chl. The transition-dipole strength of the Q_y transition of Chl-*a* has been known to depend on the refractive index of the medium.[41] We used the empirical value of 4.4 D and refractive index n of 1 according to Raszewski and Renger.[42]

We assumed here the same value of 4.4 D for the magnitude of the transition dipole of $P700^+$. This assumption seems basically consistent with the fact that the Chl cation radical in a solution showed an absorption band at around 830 nm in units of $cm^{-1}\ M^{-1}$ having a similar spectral area to that of the neutral Chl in a solution.[31,32] We do not have reliable information about the orientation of the transition-dipole vector of $P700^+$. Therefore, we calculated the values of V between each Chl oligomer and $P700^+$ with any orientations of the transition-dipole vector of $P700^+$ and then estimated its upper-limit value. Thus, the energy-transfer time τ_{ET} from each Chl oligomer to $P700^+$ was estimated here as the lower-limit value.

The spectral overlap J was calculated by using putative spectral profiles expressed by Gaussian functions

$$F_D(\nu) \text{ or } A_A(\nu) = \frac{1}{\sqrt{2\pi}\sigma} \exp\left(-\left[\frac{(\nu - \nu_0)^2}{2\sigma^2}\right]\right) \qquad (5)$$

Here, ν_0 and σ are the peak position and width of the spectra, respectively. The parameters for the fluorescence spectra of C710 and C719 were determined by fitting to $DAS_{140\ ps}$ and $DAS_{360\ ps}$, respectively. The dotted and dashed lines in Figure 7 are the simulated fluorescence spectra of C710 and C719, which are in good agreement with $DAS_{140\ ps}$ (closed triangles) and $DAS_{360\ ps}$ (closed squares), respectively. The determined parameters for the simulated fluorescence spectra are ν_0 = 13 748 cm^{-1} (727 nm) and σ = 255 cm^{-1} for C710 and ν_0 = 13,561 cm^{-1} (737 nm) and σ = 259 cm^{-1} for C719. The absorption spectrum of C719 was assumed to be the mirror image of its fluorescence spectrum and have ν_0 at 13 908 cm^{-1} (719 nm). The absorption spectrum of $P700^+$ was assumed to have the peak wavelength at 800 nm and a broad width σ of 1000 cm^{-1}. The assumed $P700^+$ absorption spectrum is consistent with that reported by Ke[30] and the spectrum of the Chl cation form in a solution.[31,32] By using the putative spectra shown in Figure 7, we obtained the values of 1.9×10^{-4}, 2.3×10^{-4}, and 9.9×10^{-4} for the spectral overlap J between C710 and $P700^+$, between C719 and $P700^+$, and between C710 and C719, respectively. In the calculation of the energy-transfer rate from red Chl to $P700^+$, we set the value of J to 2.1×10^{-4}, which is an averaged value of those between C710 and $P700^+$ and between C719 and $P700^+$.

In Table 2, we list the lower limit of the energy-transfer time τ_{ET} from each Chl oligomer to $P700^+$ estimated by the above analysis. In the present study, we adopted several assumptions for simplicity. (1) The site energy was assumed to take the same value for the all monomer Chls. (2) The dipole approximation was assumed for the excitonic interaction between the pigment molecules in an oligomer. These simplifications might result in uncertainty about the determination of the transition-dipole moment of each oligomeric Chl-*a*. Of course, we cannot expect here a quantitative agreement between the calculated and the experimentally obtained energy-transfer rates. We consider, however, that the above simulation still offers opportunities to reject the red Chl candidates that give simulated τ_{ET} severely deviated from the experimental value.

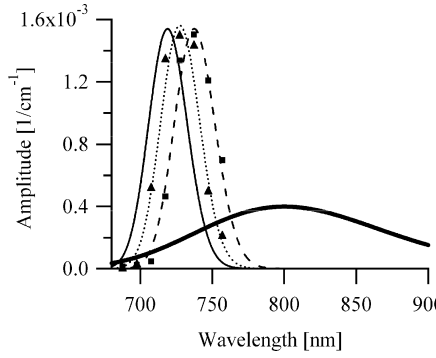

Figure 7. Putative fluorescence and absorption spectra used in the estimation of the spectral overlap J in eq 2. Dotted and dashed lines are the fluorescence spectra of C710 and C719, respectively. Thin and thick solid lines are the absorption spectra of C719 and $P700^+$, respectively. Closed triangles and closed squares show $DAS_{140\ ps}$ and $DAS_{360\ ps}$, respectively.

The present study of fluorescence dynamics showed the three red Chls having energy-transfer times to $P700^+$ of 6.1, 140, and 360 ps. According to this observation, we rejected the oligomeric Chls with predicted τ_{ET} to $P700^+$ longer than 1 ns. After this selection, seven candidates, that is, A32-B7, A33-A34, B22-B34, A24-A35, B24-B25, A26-A27, and B31-B32-B33, remained. The present experimental results also showed the existence of an energy-transfer process from one (probably C710) to another (C719) red Chl with a time constant of 170 ps. Thus, we should find a pair of Chl oligomers between which τ_{ET} is predicted to be close to 170 ps. τ_{ET} predicted among the red-Chl candidates are listed in Table S1 in Supporting Information. A pair of the red Chl candidates (A32-B7, A33-A34) gave an energy-transfer time of 66 ps, which was the closest to the experimentally obtained value of 170 ps. Thus, it was suggested that A32-B7 and A33-A34 are the most probable candidates for either C710 or C719. Damjanović et al.[20] proposed A32-B7 as the candidate for C719. Here, since a much shorter τ_{ET} to $P700^+$ was predicted for A32-B7 than for A33-A34, we assign the former to C710 and the latter to C719.

A33-A34, which was assigned to C719 above, is located near the interface of the monomer unit in the PS-I trimer. This is consistent with previous reports suggesting the proximity of C719 to the trimerization region.[14,15] Both A32-B7 and A33-A34 dimers have their transition-dipole vectors of the lower states nearly parallel to the membrane plane. This is also compatible with the observation of the linear-dichroism spectrum of PS-I of *T. elongatus* at 5 K by Schlodder et al.[43] On the other hand, this is not the case for B22-B34 and A24-A35 dimers, suggesting that these two dimers are unlikely candidates for red Chls. Another dimeric Chl pair (B24-B25, A26-A27) gave an estimated τ_{ET} of 720 ps, which was the second closest value to the experimental one. Given the considerable uncertainty in the present analysis, this pair (B24-B25, A26-A27) cannot be completely rejected from the list of candidates for C710 and C719.

We tried to determine which Chl oligomer in Table 2 can be assigned to C715 showing an ultrafast 6.1 ps energy transfer to $P700^+$. Since the fastest τ_{ET} of 46−48 ps to $P700^+$ was predicted for B24-B25 and A26-A27 in the above analysis, these dimeric Chls can be potential candidates of C715 ($C_{6.1\ ps}$). Indeed, these Chl dimers have the shortest and second-shortest distances to P700 among the candidates listed in Table 2. However, the predicted τ_{ET} were still an order of magnitude longer than that obtained experimentally. We, thus, cannot give a concrete explanation for this discrepancy.

There is almost no Chl giving a sufficiently high V value to achieve the energy-transfer time of 6.1 ps to $P700^+$. The only exceptions to this are Chls forming the electron-transfer chain at the center of PS-I. We speculate here that the involvement of these central Chls in the energy-transfer path might be the key mechanism to explain the extremely fast energy transfer of $C_{6.1\ ps}$. The excited state of $C_{6.1\ ps}$ might be delocalized over a wider region than assumed above. If the delocalization extends to the central Chls, a very fast energy transfer to $P700^+$ is expected. In this case, we might be better to apply the generalized Förster theory proposed by Sumi et al.,[44,45] which might further enhance the energy-transfer rate. Even though the central Chls are not involved in $C_{6.1\ ps}$ excited state, they can mediate the energy transfer from $C_{6.1\ ps}$ to $P700^+$ as a quantum-mechanical virtual state, as proposed by Sumi to explain the energy-trapping mechanism from the purple bacterial light-harvesting complex to the reaction center.[46] This superexchange mechanism might be another possible explanation for the ultrafast energy transfer of $C_{6.1\ ps}$.

We can raise another question about the energy-transfer kinetics of $C_{6.1\ ps}$. As illustrated in Figure 6A, the present study revealed an extremely rapid energy funneling from 60 bulk Chls into $C_{6.1\ ps}$ within at most 1.3 ps in PS-I with $P700^+$. It should be questioned whether this rapid funneling into $C_{6.1\ ps}$ is achieved by sequential energy migrations among 60 molecules. If the Förster mechanism is assumed, such a rapid funneling requires not only very fast energy transfers between individual Chls but also a quite effective arrangement of the excited-state energy levels of individual Chls that is smoothly biased toward $C_{6.1\ ps}$. Instead, the formation of the delocalized pigment domains might be the key mechanism of the ultrafast energy funneling into $C_{6.1\ ps}$. Since Chls in PS-I are coupled by quite strong excitonic interactions with each other, it is quite likely that excited states are delocalized over a large number of Chls at cryogenic temperature. In fact, Gibasiewicz et al. have suggested the formation of delocalized exciton over the 6−8 Chls at the central part of PS-I[47,48] on the basis of their results of the femtosecond transient absorption measurement at cryogenic temperature. Further investigation about the delocalization of the excited state in PS-I is needed.

Conclusions

The present study revealed the kinetic aspect of red Chls over the subpicosecond to the nanosecond time range at cryogenic temperature. We found three kinetically different red Chls, $C_{6.1\ ps}$, $C_{140\ ps}$, and $C_{360\ ps}$ that have energy-transfer times to an oxidized P700 of 6.1, 140, and 360 ps, respectively. $C_{6.1\ ps}$, $C_{140\ ps}$, and $C_{360\ ps}$ were assigned to C715, C710, and C719 based on the peak wavelength of the DAS components, respectively. It was shown that light harvesting through $C_{6.1\ ps}$ is the main path of the energy trapping to $P700^+$, while the direct energy transfer to P700 becomes the main path to a neutral P700.

On the basis of the simulation of the energy-transfer times, $C_{140\ ps}$ (C710) and $C_{360\ ps}$ (C719) were assigned to the dimeric Chls, A32-B7 and A33-A34, respectively. Although the estimated energy-transfer time to $P700^+$ was much longer than the observed value of 6.1 ps, the dimeric Chls B24-B25 and A26-A27 were considered potential candidates for $C_{6.1\ ps}$ (C715). We could not give a concrete explanation for the energy-transfer dynamics of $C_{6.1\ ps}$. Even though significant uncertainty was involved in our analysis, the deviation between the predicted and the experimental energy-transfer times from $C_{6.1\ ps}$ to $P700^+$ is still considered too large. The mechanism of the ultrafast energy funneling into $C_{6.1\ ps}$ still remains to be studied. Our knowledge about the excited state of pigment in PS-I at cryogenic temperature does not seem to be sufficient to understand the light-harvesting dynamics of $C_{6.1\ ps}$. More quantitative study of the delocalization of the excited state in PS-I is an important future issue.

Acknowledgment. The work was supported in part by Grants-in-Aid for Scientific Research (No. 17750010), the 21st COE program for "the origin of the universe and matter" from the Japanese Ministry of Education, Science, Sports, and Culture (MEXT), and the Japan Society for the Promotion of Science (JSPS). Y.S. thanks Chihiro Kamidaki for sample preparation, Ayaka Hasegawa for analysis of blue-native gel electrophoresis, and Dr. Akihiro Kimura for stimulating discussions.

Supporting Information Available: This material is available free of charge via the Internet at http://pubs.acs.org.

References and Notes

(1) Golbeck, J. H. In *The Molecular Biology of Cyanobacteria*; Bryant, D. A., Ed.; Kluwer Academic Publishers: Dordrecht, 1994; pp 319−360.
(2) Diner, B. A.; Babcock, G. T. In *Oxygenic Photosynthesis: The Light Reactions*; Ort, D. R., Yocum, C. F., Eds.; Kluwer Academic Publishers: Dordrecht, 1996; p 13.
(3) Jordan, P.; Fromme, P.; Witt, H. T.; Klukas, O.; Saenger, W.; Krauss, N. *Nature* **2001**, *411*, 909–917.
(4) Ben-Shem, A.; Frolow, F.; Nelson, N. *Nature* **2003**, *426*, 630–635.
(5) Watanabe, T.; Kobayashi, M.; Hongu, A.; Nakazato, M.; Hiyama, T.; Murata, N. *FEBS Lett.* **1985**, *191*, 252–256.
(6) Holzwarth, A. R. *Biophysical Techniques in Photosynthesis. Advances in Photosyntheses Researches*; Kluwer Academic Publishers: Dordrecht; 1996.
(7) Holzwarth, A. R.; Muller, M. G.; Niklas, J.; Lubitz, W. *J. Phys. Chem. B* **2005**, *109*, 5903–5911.
(8) Holzwarth, A. R.; Schatz, G.; Brock, H.; Bittersmann, E. *Biophys. J.* **1993**, *64*, 1813–1826.
(9) Melkozernov, A. N.; Lin, S.; Blankenship, R. E. *Biochemistry* **2000**, *39*, 1489–1498.
(10) Slavov, C.; Ballottari, M.; Morosinotto, T.; Bassi, R.; Holzwarth, A. R. *Biophys. J.* **2008**, *94*, 3601–3612.
(11) Croce, R.; Dorra, D.; Holzwarth, A. R.; Jennings, R. C. *Biochemistry* **2000**, *39*, 6341–6348.
(12) Savikhin, S.; Xu, W.; Martinsson, P.; Chitnis, P. R.; Struve, W. S. *Biochemistry* **2001**, *40*, 9282–9290.
(13) Gobets, B.; van Stokkum, I. H. M.; van Mourik, F.; Dekker, J. P.; van Grondelle, R. *Biophys. J.* **2003**, *85*, 3883–3898.
(14) Pålsson, L. O.; Dekker, J. P.; Schlodder, E.; Monshouwer, R.; van Grondelle, R. *Photosynth. Res.* **1996**, *48*, 239–246.
(15) Rätsep, M.; Johnson, T. W.; Chitnis, P. R.; Small, G. J. *J. Phys. Chem. B* **2000**, *104*, 836–847.
(16) Zazubovich, V.; Matsuzaki, S.; Johnson, T. W.; Hayes, J. M.; Chitnis, P. R.; Small, G. *J. Chem. Phys.* **2002**, *275*, 47–59.
(17) Melkozernov, A. N.; Lin, S.; Blankenship, R. E.; Valkunas, L *Biophys. J.* **2001**, *81*, 1144–1154.
(18) Byrdin, M.; Jordan, P.; Krauss, N.; Fromme, P.; Stehlik, D.; Schlodder, E *Biophys. J.* **2002**, *83*, 433–457.
(19) Sener, M. K.; Lu, D. Y.; Ritz, T.; Park, S.; Fromme, P.; Schulten, K. *J. Phys. Chem. B* **2002**, *106*, 7948–7960.
(20) Damjanović, A.; Vaswani, H. M.; Fromme, P.; Fleming, G. R. *J. Phys. Chem. B* **2002**, *106*, 10251–10262.
(21) Balaban, T. S. *FEBS Lett.* **2003**, *545*, 97–102.
(22) Jelezko, F.; Tietz, C.; Gerken, U.; Wrachtrup, J.; Bittl, R. *J. Phys. Chem. B* **2000**, *104*, 8093–8096.
(23) Byrdin, M.; Rimke, I.; Schlodder, E.; Stehlik, D.; Roelofs, T. A *Biophys. J.* **2000**, *79*, 992–1007.
(24) Slavov, C.; El-Mohsnawy, E.; Rögner, M.; Holzwarth, A. R. *Chem. Phys.* **2009**, *357*, 163–170.
(25) Pålsson, L. O.; Flemming, C.; Gobets, B.; van Grondelle, R.; Dekker, J. P.; Schlodder, E. *Biophys. J.* **1998**, *74*, 2611–2622.
(26) Komura, M.; Shibata, Y.; Itoh, S. *Biochim. Biophys. Acta* **2007**, *1757*, 1657–1668.
(27) Kennis, J. T. M.; Gobets, B.; van Stokkum, I. H. M.; Dekker, J. P.; van Grondelle, R.; Fleming, G. R. *J. Phys. Chem. B* **2001**, *105*, 4485–4494.
(28) Shibata, Y.; Kawamoto, S.; Satoh, Y.; Itoh, S. *Photosynth. Res.* **2007**, *91*, 143–143.
(29) Shibata, Y.; Murai, Y.; Satoh, Y.; Fukushima, Y.; Kajima, K.; Ikeuchi, M.; Itoh, S. *J. Phys. Chem. B* **2009**, *113*, 8192–8198.
(30) Ke, B. *Arch. Biochem. Biophys.* **1972**, *152*, 70–77.
(31) Davis, M. S.; Forman, A.; Fajer, J. *Proc. Natl. Acad. Sci. U.S.A.* **1979**, *76*, 4170–4174.
(32) Chauvet, J. P.; Vlovy, R.; Santus, R.; Land, E. J. *J. Phys. Chem.* **1981**, *85*, 3449–3456.
(33) Fromme, P.; Witt, I. *Biochim. Biophys. Acta* **1998**, *1365*, 175–184.
(34) Kawakami, K.; Iwai, M.; Ikeuchi, M.; Kamiya, N.; Shen, J. R. *FEBS Lett.* **2007**, *581*, 4983–4987.
(35) Heathcote, P.; Hanley, J. A.; Evans, M. C. W. *Biochim. Biophys. Acta* **1993**, *1144*, 54–61.
(36) Sétif, P.; Bottin, H. *Biochemistry* **1989**, *28*, 2689–2697.
(37) Brettel, K. *Biochim. Biophys. Acta* **1997**, *1318*, 322–373.
(38) Riley, K. J.; Reinot, T.; Jankowiak, R.; Fromme, P.; Zazubovich, V. *J. Phys. Chem. B* **2007**, *111*, 286–292.
(39) Pullerits, T.; Hess, S.; Herek, J. L.; Sundström, V. *J. Phys. Chem. B* **1997**, *101*, 10560–10567.
(40) Renger, T.; May, V.; Kühn, O. *Phys. Rep.* **2001**, *343*, 137–254.
(41) Knox, R. S.; Spring, B. Q. *Photochem. Photobiol.* **2003**, *77*, 497–501.
(42) Raszewski, G.; Renger, T. *J. Am. Chem. Soc.* **2008**, *130*, 4431–4446.
(43) Schlodder, E.; Shubin, V. V.; El-Mohsnawy, E.; Roegner, M.; Karapetyan, N. V. *Biochim. Biophys. Acta* **2007**, *1767*, 732–741.
(44) Sumi, H. *J. Phys. Chem. B* **1999**, *103*, 252–260.
(45) Mukai, K.; Abe, S.; Sumi, H. *J. Phys. Chem. B* **1999**, *103*, 6096–6102.
(46) Sumi, H. *J. Phys. Chem. B* **2002**, *106*, 13370–13383.
(47) Gibasiewicz, K.; Ramesh, V. M.; Lin, S.; Woodbury, N. W.; Webber, A. N. *J. Phys. Chem. B.* **2002**, *106*, 6322–6330.
(48) Gibasiewicz, K.; Ramesh, V. M.; Lin, S.; Redding, K.; Woodbury, N. W.; Webber, A. N. *Biophys. J.* **2003**, *85*, 2547–2559.

JP909583R